5-2019

A Low-Cost Search-and-Rescue Drone Platform

Jonathan McClure
jmm3848@rit.edu

A Low-Cost Search-and-Rescue Drone Platform

by

Jonathan McClure

A thesis submitted in partial fulfillment of the requirements for the
Degree of Master of Science in Electrical Engineering

Supervised by

Professor Dr. Ferat Sahin

Department of Electrical and Microelectronic Engineering
Kate Gleason College of Engineering
Rochester Institute of Technology
Rochester, New York
May 2019

Approved by:

Dr. Ferat Sahin, Thesis Advisor Date
Professor, Department of Electrical and Microelectronic Engineering

---

Dr. Raymond Ptucha, Committee Member Date
Assistant Professor, Department of Computer Engineering

Dr. Sohail Dianat, Committee Member Date
Department Head, Department of Electrical and Microelectronic Engineering

---

Dr. Sohail Dianat, Department Head Date
Department Head, Department of Electrical and Microelectronic Engineering

Acknowledgments

I would like to thank Dr. Ferat Sahin for serving as advisor. Without his support and guidance, this project would never have gotten off the ground.

I would also like to thank the members of the Multi-Agent Biorobotics Lab research group, especially Celal Savur, Shitij Kumar, and Anmol Modur, for their helpful feedback and advice. I am also grateful to Caleb Guillaume, Aaron Reckless, Chris Ugras, and Matthew Williams for their assistance with the testing process.

Finally, I would like to thank my family and friends for their enduring support and encouragement.

Dedication

This thesis is dedicated to my parents. Thank you for all of your love and support, and for teaching me the value of hard work and perseverance.

Abstract

A Low-Cost Search-and-Rescue Drone Platform

Jonathan McClure

Supervising Professor: Dr. Ferat Sahin

In this work, an unmanned aerial system is implemented to search an outdoor area for an injured or missing person (subject) without requiring a connection to a ground operator or control station. The system detects subjects using exclusively on-board hardware as it traverses a predefined search path, with each implementation envisioned as a single element of a larger swarm of identical search drones. To increase the affordability of such a swarm, the system cost per drone serves as a primary constraint. Imagery is streamed from a camera to an Odroid single-board computer, which prepares the data for inference by a Neural Compute Stick vision accelerator. A single-class TinyYolo network, trained on the Okutama-Action dataset and an original Albatross dataset, is utilized to detect subjects in the prepared frames. The final network achieves 7.6 FPS in the field (8.64 FPS on the bench) with an 800x480 input resolution. The detection apparatus is mounted on a drone and field tests validate the system feasibility and efficacy.

List of Contributions

- Assembly of a drone capable of autonomous flight and identification of persons on the ground, at a total cost less than the market entry price for conventional search-and-rescue drones.
- Implementation of entirely onboard, on-the-edge inferencing at data rates and resolutions beyond those of comparable systems.
- Creation and labelling of a custom dataset for identification of subjects in high-angle aerial photography.
- Successful field tests showing system capability of entirely autonomous detection of missing persons.
- J. McClure, F. Sahin, "A Low-Cost Search-and-Rescue Drone for Near Real-Time Detection of Missing Persons," *System of Systems Engineering (SoSE), 14th International Conference on*, 2019. Accepted for publication.

Contents

List of Figures

List of Tables

Chapter 1

Introduction

Use of drones for search-and-rescue, surveillance, or related tasks typically requires that imagery recorded by the drone be streamed to a ground control station (GCS) for processing, with some associated latency. Alternatively, the imagery may be saved onboard the drone and retrieved for offline processing when the flight is complete [1]. The latter case introduces too much delay to be of use in a search-and-rescue application. Streaming solutions work well for a single drone [2]; however, when the number of drones is scaled up (such as in a search swarm [3]), the GCS may struggle to perform simultaneous inferencing on every stream. Depending on the hardware capabilities of the device, the demands of multiple agents could overwhelm the GCS, introducing inference latency issues or potentially even resulting in dropped frames. The data could be relayed to a distant processing station with more computing resources, but depending on the remoteness of the search area sufficient infrastructure may not be in place to facilitate this.

Implementations of deep learning networks at-the-edge must balance accuracy and throughput requirements against power consumption. In the same manner, the use of drones for search-and-rescue in large outdoor areas carries an intrinsic need for low power use, in order to maximize flight time and thus cover more search area [4]. The use of a vision accelerator such as the Movidius Neural Compute Stick (NCS) in conjunction with a single-board computer has been shown to extend system capabilities while maintaining a low power profile and low cost [5]. The NCS thus presents an ideal means by which to implement onboard inferencing in a drone-based search-and-rescue application. Its small size and 1W power envelope [6] mean it can be deployed onboard a drone and used to perform inference on drone imagery, without significantly taxing system resources. This greatly reduces the quantity of information to be communicated to the GCS - rather than a continuous video feed, only the inference results need be transmitted. This reduces the stress upon the machine, while also allowing its administrator, the Remote Pilot in Command (RPIC), to focus on other tasks rather than providing individualized oversight for each feed.

In this work, a NCS vision accelerator is used with a SBC aboard a low-cost, purpose-built drone. An object detection network running on the accelerator is used to detect subjects on the ground through imagery recorded onboard. The system is shown through field testing to provide a viable platform for the automated detection of missing persons in outdoor areas.

The remainder of this paper is structured as follows. Chapter 2 explores related works. Chapters 3 and 4 explores the hardware and software elements of the final system implementation. Chapter 5 presents both bench and field test results for the system and its missing person detection network. Chapters 6 and 7 provide final conclusions and suggestions for future work.

Chapter 2

Related Works

In search-and-rescue scenarios, search teams are often forced to make use of helicopters or other aircraft to scout terrain for missing persons [7]. The operating costs for helicopters have been reported by various sources as ranging from $1600 to $16,500 per hour USD [8] [9]. The use of unmanned search aircraft such as drones may potentially result in a lower cost per search than the use of helicopters or search planes, in addition to decreasing the time required to find a subject [10].

The minimization of cost in drone design for search-and-rescue applications has been touched upon in the literature [11]. Reference [12] propose a "smart" detection system to be mounted on a drone that utilizes passive infrared (PIR) sensors to detect humans. However, the range and field-of-view limitations of such sensors, as well as their inability to distinguish human triggers from animals, make them ill-suited for an outdoor search over a large area. A search-and-rescue drone was implemented by [13], but at a high unit cost and with a focus on interiors and small sites.

The literature extensively covers the path-planning aspects of search-and-rescue for drones [4], including multi-agent implementations [14]. In fact, [3] suggest as future work that such collaborative systems could be implemented onboard drones using SBCs. The findings of [15] suggest a Bluetooth Low-

Energy LoRa modem may be used to connect SBCs across significant distances despite a low unit cost. To further extend the effective range of search drones, [16] propose and verify through simulation a method by which a master drone can relay messages to slave drones at great distances from the GCS. Means of notifying operators when subjects have been found by the search drone or drones are addressed by [17] and [2].

While the use of a thermal camera has been shown to improve subject detection rates [2], low-cost thermal solutions lack sufficient resolution to present enough detail for high-angle detection [18]. Additionally, no publicly accessible dataset of high-angle thermal imagery is available for use, meaning the functionality could not be trained into a detection network without requiring an extensive custom dataset. Aerial images present a high-angle, often oblique view of subjects on the ground [19]. Conversely, conventional pedestrian datasets such as [20] feature subjects at approximately the same elevation as the camera. Further complications result from the small size (in pixels) of subjects in aerial imagery, compared to most pedestrian datasets in which the subjects appear much larger in proportion to the image size. A noteable exception is the Okutama-Action dataset [21], featuring high-angle video sequences shot from drones and showing multiple actors in various poses.

The potential of the NCS vision accelerator has been explored in the literature, in applications ranging from embedded road condition monitoring [22] to detection of defects in semiconductor laser chips [23]. Drone manufacturer DJI utilizes the same chip used in the NCS in their DJI Spark miniature drone to facilitate gesture sensing, obstacle avoidance, and facial recognition [24]. The most common platform utilized in the literature consists of a single NCS or several NCS devices for inference, plugged into a Raspberry Pi single-board computer (SBC) [23] [25] [22] [26]. The performance of networks on parallel NCS devices have been shown to scale (mostly) uniformly with the number of devices used [6]. While other authors have noted the possibility that the use of USB2 ports limits the rate at which the NCS can load and transmit data [27], an empirical analysis of the effects of USB transfer rate on the platform's performance has not yet been reported. Additionally, the potential of the second generation NCS (NCSv2) has yet to be explored.

Chapter 3

System Hardware

When selecting components with which to build the drone, cost had to be balanced with quality to ensure the system was not only inexpensive but also reliable and robust. Some components utilized here would not be recommended for use in future implementations, should another unit be constructed. Section 3.1 explores the components essential for flight of the drone itself, while Section 3.2 explores the peripherals required to implement the onboard missing person detection system. Section 3.3 summarizes the hardware utilized and associated cost.

3.1 Drone Hardware

The drone utilizes brushless DC motors that provide sufficient thrust to support a total payload (components included) of at least 800g, with a recommended upper bound of 1600g. This wide range depends on such factors as battery voltage, atmospheric conditions, temperature, and other factors [28]. Four separate electronic speed controllers (ESCs) are utilized to provide completely individualized three-phase control of each motor. Fig. 3.1 shows the mounting of these components on the frame arms. The ESC is not conventionally secured; instead, its wiring is snaked through the gaps in the arm and

Figure 3.1: A motor and ESC viewed from below.

the resulting friction holds it in place.

Dual 3-cell (3s) 1800mAh-capacity LiPo batteries, with discharge rate of 75C each, provide power for the various onboard systems at 11.1V nominal (11.4V actual when fully charged). The parallel combination of the batteries facilitates a peak discharge current of 270A. Each motor is capable of up to 15.1A current draw under duress. The flight controller and connected peripherals require approximately 1.5A at boot and 1A in flight. The Odroid may require up to 6A current when preforming intensive computation, not including the approximately 500mA draw of the NCS. Therefore, the maximum total current needs of the system may thus be approximated as 68A - well below the maximum capacity supported.

As the ESCs support either 11.1V or 14.8V (4s) drive, 3s batteries were chosen to save weight. While the drone has been tested and shown to be flight capable using only a single battery, it may consume power rapidly when performing inferences in flight due to the additional draw of the Odroid. There-

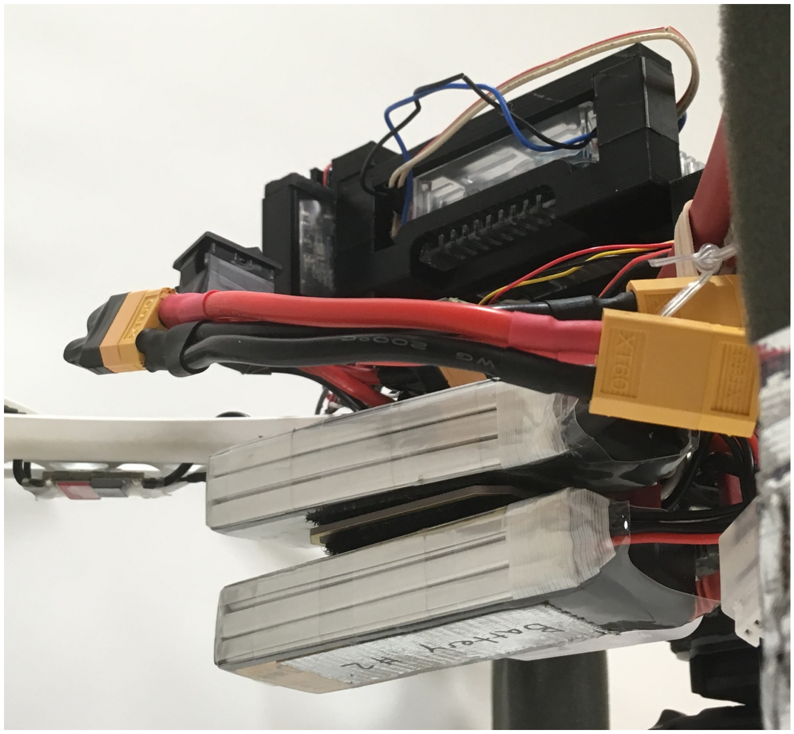

Figure 3.2: While the parallel combination of two LiPo batteries extends the flight time of the system, a better solution for future implementations would be a single battery with a higher capacity.

fore, to provide insurance against undervoltage conditions and to permit multiple consecutive flights without requiring the battery to be swapped, two batteries are instead mounted in parallel to effectively double the flight time of the system (Fig. 3.1). For future implementations, it is suggested that a single battery with a larger capacity be utilized, extending the possible flight time without the additional weight penalty associated with adding a second battery.

A toggle switch implemented at the batteries' connectors permits them to be disconnected and the system powered down without requiring they be physically unplugged. The switch output is connected, in parallel, to a power distribution board (PDB), power module (PM), and universal battery eliminator circuit (UBEC). These are shown in Fig. 3.4. The PDB is simply used as the connection point for each of the ESCs, providing a direct connection to the 11.1V rail to drive the motors. The PM provides a clean 5V rail to the FC while supporting voltage and current monitoring of the batteries; the FC in turn routes that rail to the Teensy, GPS, and onboard telemetry and control radios. The UBEC provides another clean 5V rail for use by the Odroid and in turn the NCS. The isolation of the two 5V rails prevents load spikes due to the Odroid from adversely affecting the FC and other onboard components. Fig. 3.3 shows the different voltage rails present in the system.

A PixHawk Mini fulfills the role of flight controller (FC), aggregating data from the GPS, ESC feedback, and internal barometer and accelerometer to facilitate autonomous flight between waypoints. The unit was selected for its small footprint and low price point; its only limiting factor is the presence of only one UART port, whereas its full-size counterpart (the Pixhawk) has several available ports but a larger footprint and weight. The primary function of the UART port is to facilitate communicate with a ground control station (GCS) by sending MavLink messages via a telemetry radio.

With the Pixhawk Mini, in order for a device such as an onboard computer to interface with the FC, the UART bus must be hijacked. A Teensy 3.1 microcontroller serves as a man-in-the-middle to relay messages between the various system endpoints (Fig. 3.5a). The Teensy typically acts as a FIFO

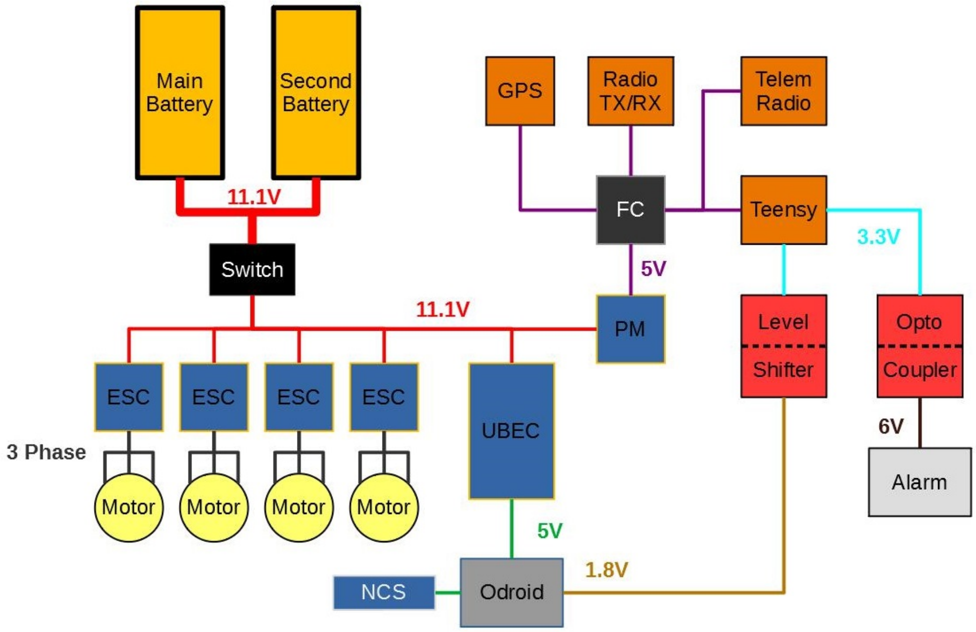

Figure 3.3: System power flow and voltage rail diagram. Buses of the same color are referenced to the same voltage source and share a return path.

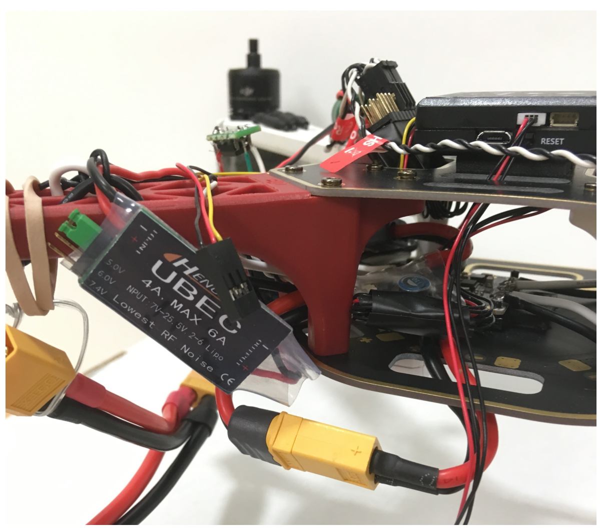

Figure 3.4: The UBEC, PM are used to rectify the 11.1V battery rails down to clean 5V lines, while the PDB passes the battery rail to the ESCs directly.

buffer for the MavLink messages between the FC and GCS. If an incoming message from the Odroid were detected, then the next time the bus was quiet this message would be sent to the FC; essentially, the onboard computer thus mimics a GCS for the purpose of sending a command. The additional UART ports of the full-size Pixhawk would easily permit connections to secondary devices such as the onboard computer via an FTDI cable without requiring this man-in-the-middle; therefore, it is recommended over the Pixhawk Mini for future implementations in which the flight controller and onboard computer must interface with each other.

For this implementation, computer-to-FC communication support is implemented as proof of concept but not utilized in-flight. Instead, the UART GPIO of the computer are repurposed to pass an alarm control signal to the Teensy, which in turn utilizes it as the input for the drive circuitry of an optocoupler (Fig. 3.5b). This provides isolated control of an alarm buzzer mounted below the frame, permitting the implementation of auditory feedback to indicate error conditions or successful detection of subjects.

Although the FC ships with the PX4 autopilot system, this implementation instead utilizes ArduPilot as its autopilot environment. The latter often exhibits better performance and stability when attempting to "loiter", or hold a fixed position, in windy conditions. Of the flight modes supported by ArduPilot, three are utilized in this application - Stabilize, AltHold, and Auto. Stabilize is characterized by entirely manual control of the throttle, roll, pitch, and yaw. In AltHold mode, the throttle is primarily controlled by the autopilot; when the throttle stick is centered, the drone will hold its

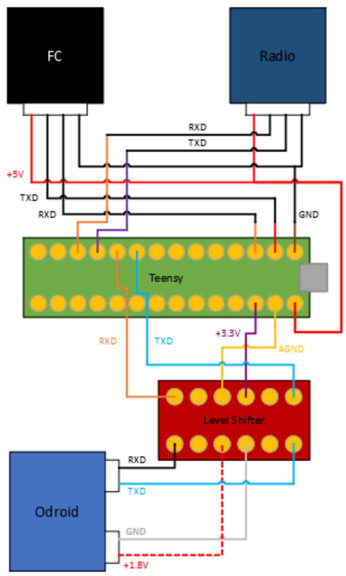

(a) Serial man-in-the-middle

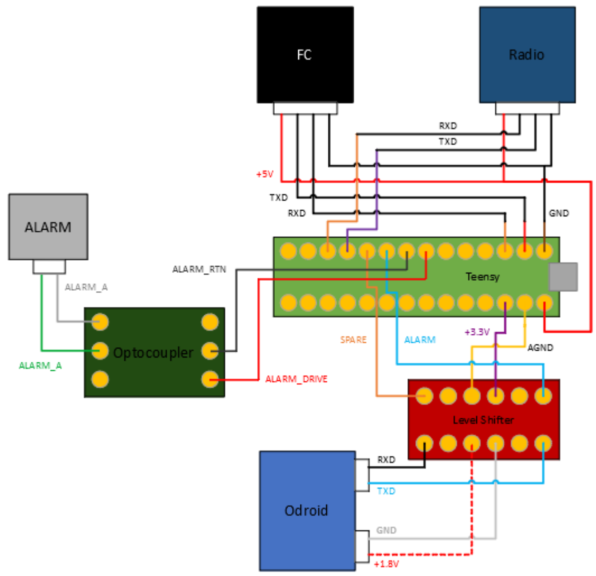

(b) Alarm control

Figure 3.5: Teensy wiring diagrams

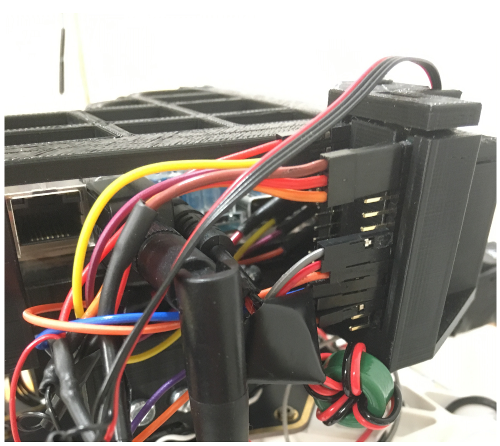

(a) A 3D-printed mount protects the Teensy while providing easy access to GPIO for prototyping.

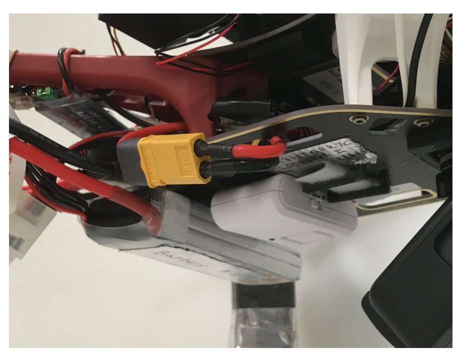

(b) A 120dB alarm system (forward of battery) provides auditory feedback to the operator via the Teensy.

Figure 3.6: Teensy implementation

current altitude, while increasing or decreasing the throttle out of the 40-60% "dead zone" will cause the drone to ascend or descend correspondingly. The "Auto" mode is characterized by essentially fully autonomous operation; the operator can control the yaw to rotate the drone if desired, but the roll, pitch, and throttle are entirely controlled by the autopilot. Auto mode will execute a series of commands stored as a "mission". Some pertinent commands employed in this application include takeoff and landing sequences, navigation to waypoints, and timed loitering.

The Auto navigation mode is facilitated by the presence of an onboard GPS unit. The mode may only be utilized when the GPS has a connection to at least four satellites and the extended Kalman filter (EKF) utilized for position estimation has sufficiently stabilized. For best results, the GPS is mounted in a forward position such that nothing impedes its "view" of the sky. The UBEC, PM, and batteries are placed as far away from the GPS unit as possible to reduce possible electromagnetic interference. A custom 3D-printed case and mount are utilized to secure and protect the unit. As care should be taken to avoid surrounding the unit with metal components that might potentially block RF signals, nylon screws are employed for mounting purposes (Fig. 3.7).

A 2.4GHz 9-channel transmitter and receiver facilitate manual control of the drone for safety and accessibility reasons. One three-position switch is utilized to switch between the flight modes of the FC. Another two-position switch is mapped to the emergency motor stop function. The remaining switches on the controller are unused; as such, in future implementations a simplified con-

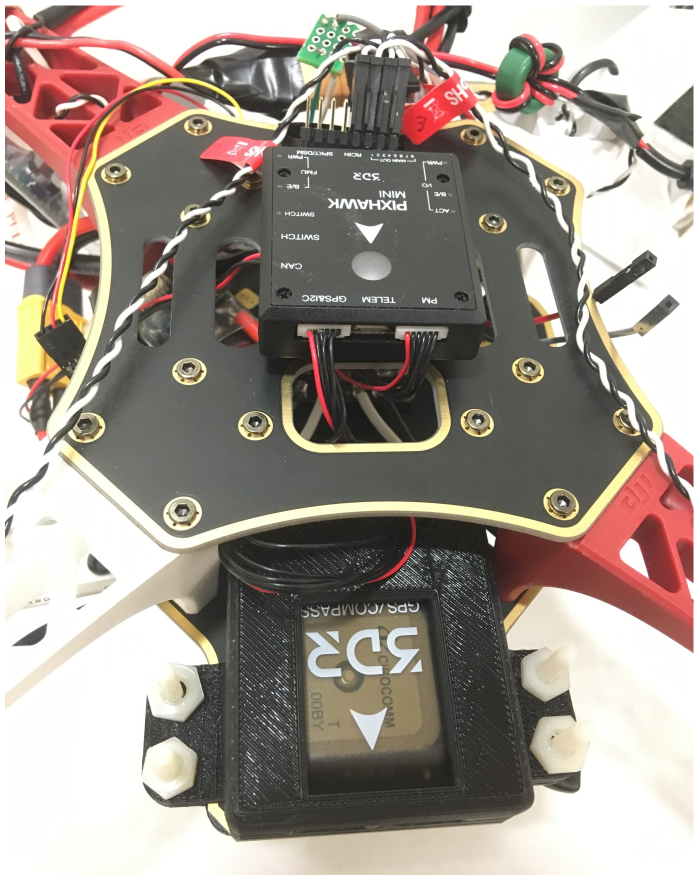

Figure 3.7: The FC is mounted at the drone's center of gravity atop foam blocks, which isolate the internal accelerometer and gyroscope from vibrations in the airframe. The GPS is mounted forward and as far away from the power circuitry as possible.

troller with fewer channels may instead be utilized, in order to reduce costs. If the antenna is allowed to dangle, it nearly touches the DC lines to the PM - an undesirable source of interference that has been observed to cause a loss of connection between the drone and controller. Thus, in order to reduce this noise, a mast is utilized to secure the receiver antenna and direct it upwards.

To support monitoring of the drone flight systems, as well as uploading of waypoint coordinates, Mission Planner is utilized as the system GCS, running offboard on a laptop. It connects to the flight controller via the telemetry radio (note that in this implementation, all traffic is routed through the Teensy). If the drone loses the connection to the GCS, it will continue its flight regardless. However, if the drone loses its connection to the operator's controller, it will return to its takeoff point and perform a landing there, in order to prevent potential flyways. This behavior is configurable, meaning operation completely independent of a ground station and ground operator connection is possible.

In its entirety, the system weighs in at 1.50kg, near the upper bound of the suggested 800g-1600g payload range. Primary contributors include 150g from each of two batteries, 230g from the motors, 280g from the frame, 170g from the camera and mount, and 140g for the Odroid and NCS. Other than the frame itself, all mounting components were custom-designed in SolidWorks. A Monoprice Mini (Fig. 3.8) was utilized to 3D print the mounts out of PLA plastic. Together, these components constitute a significant portion of the remaining system weight. Additional improvements include the use of foam blocks to extend the drone legs and cushion against ground impacts during landing operations.

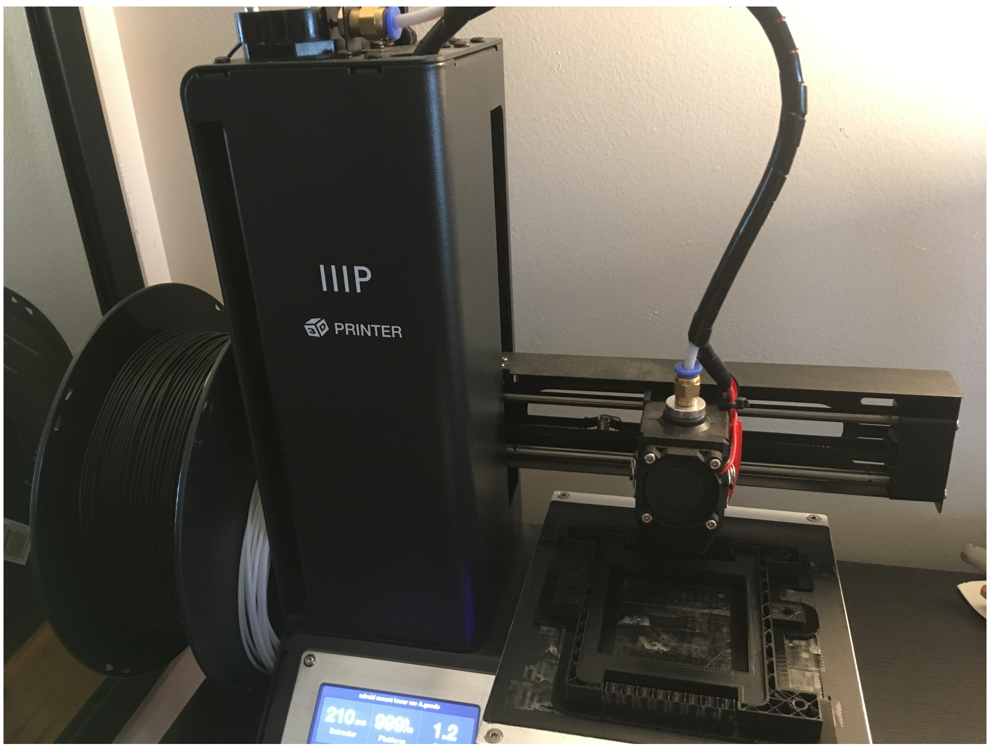

Figure 3.8: A Monoprice Mini was utilized to 3D print custom mounting components out of PLA. Here, it is seen here printing the lower Odroid mount, which requires a support structure due to its overhanging crossbar.

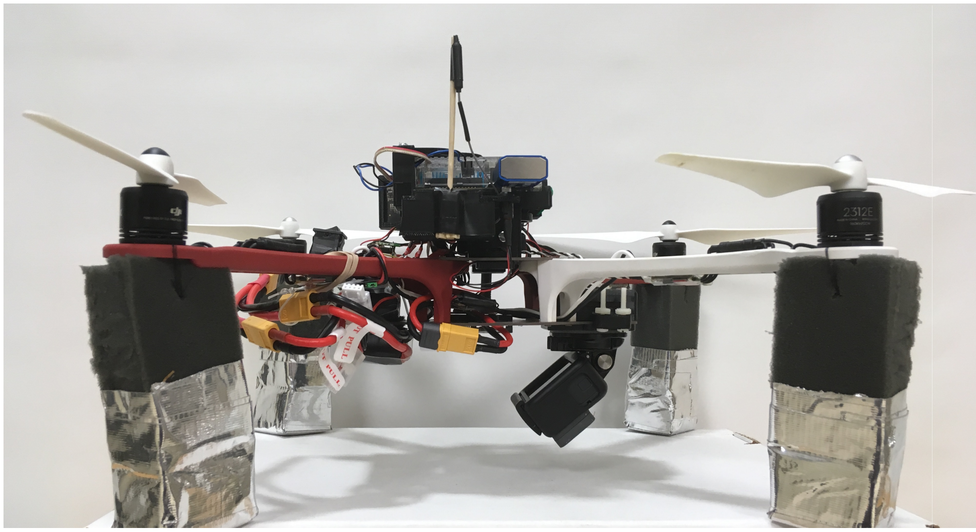

Figure 3.9: With both the main and secondary batteries and camera equipped, the drone measures a considerable 1.5kg. In future implementations, care should be taken to keep weight down in order to prolong flight time.

3.2 Hardware for Onboard Detection of Subjects

At the heart of the onboard processing system is the Odroid XU-4 single-board computer (SBC). It features 2Gb of available RAM, both Cortex-A15 (2Ghz) and Cortex-A7 (1.2Ghz) quad-core CPUs, and dual USB3 ports in addition to a single USB2 port [29]. While the Odroid requires a minimum of 2A to boot, for best performance a 6A-capable 5V power supply is recommended; here, this role is fulfilled by the 6A UBEC. The unit used in this implementation runs a MATE graphical desktop environment over the Ubuntu 16.04 operating system. In the field, an Ethernet cable is employed to connect the SBC to a laptop running an SSH client. Once the search-and-rescue program code has been initialized, the cable may be removed.

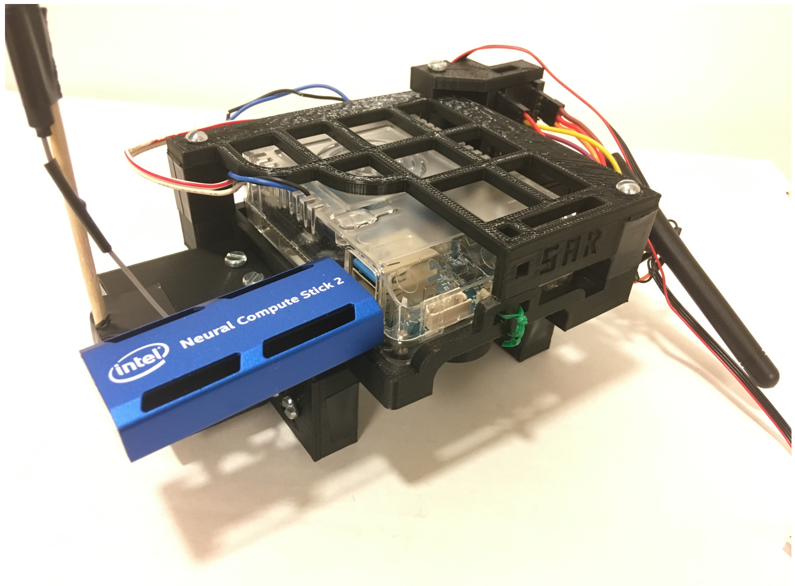

Figure 3.10: Odroid and NCS

An Intel Neural Compute Stick (NCS) vision accelerator is utilized to load the object detection network and perform inferences on images. Each NCS makes use of an embedded vision processing unit (VPU) for network calculations. The device is interfaced with through a USB port, with support for USB3 data transfer rates.

The Neural Compute Stick (NCSv1) utilizes a Movidius Myriad v2 VPU with 12 Streaming Hybrid Architecture Vector Engine (SHAVE) cores [30]. Networks are deployed via the Neural Compute Software Development Kit (NCSDK) in the form of graph files. Alternatively, the OpenVINO toolkit may be utilized for deployment of networks as Intermediate Representation (IR) files. A recently released improved version, the Neural Compute Stick 2 (NCSv2), features a Myriad X VPU with 16 SHAVE cores. Unlike the NCSv1, the device is only compatible with the OpenVINO toolkit. The NCSv2 is advertised as capable of up to eight times the performance of the NCSv1 [31].

As both the NCSv1 and NCSv2 are fanless, if the device experiences significant stress (such as high throughput or extended use), it is prone to overheating. This can result in the connection between the Odroid and the device closing unexpectedly. While this issue has been observed extensively on the bench, under flight conditions the airflow over the device helps to cool it and reduce the risk of overheating. A similar problem manifests when the device becomes too cold, such as when performing extensive field testing in temperatures below freezing. Attaching air-activated hand warmers near the NCS has been observed to reduce or eliminate temperature-related device shutdowns in cold weather conditions.

A GoPro Hero 6 is utilized as the main onboard camera for the system, chosen for its integrated stabilization (eliminating the need for a gimbal) and durability. While the mount for the camera (Fig. 3.11) is rugged and reliable, it prevents access to the camera's HDMI and USB ports. Therefore, the streaming capabilities of the camera over WiFi are exploited. A WiFi antenna module plugged into the USB2 port of the Odroid provides a connection to the wireless hotspot of the camera.

A cheaper, less-featured camera could easily be substituted to save costs in future implementations. However, as the motors may induce vibrations on the airframe under flight conditions, video stabilization techniques may be required. These could be implemented via software, utilizing techniques such as point feature matching with OpenCV, or in hardware through the use of

Figure 3.11: GoPro, mounted on the forward underside of the drone

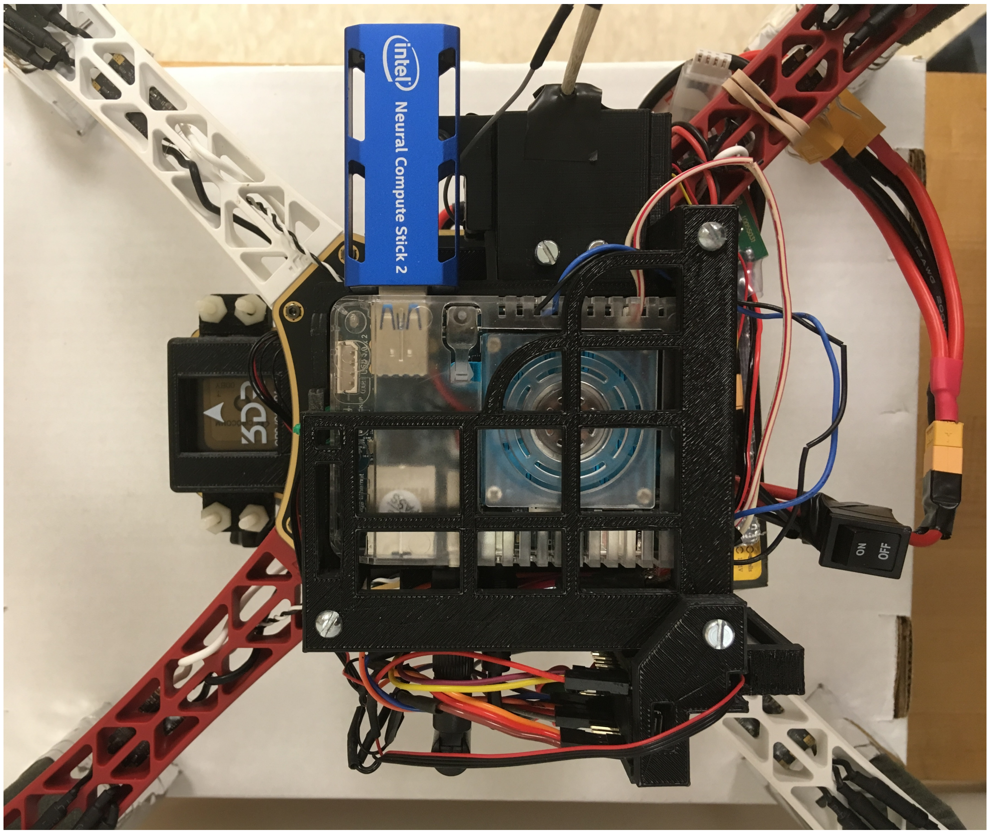

Figure 3.12: The 3D-printed mount architecture was designed to have as small a footprint as possible, in order to avoid interference with or risk of collision between the propellers and the devices.

a gimbal. The gimbal carries its own drawbacks, such as increased system weight and cost. If a wireless network is to be utilized for drone-to-drone communication in future swarm implementations, a hardwired camera should be implemented to free up the Odroid to network connections.

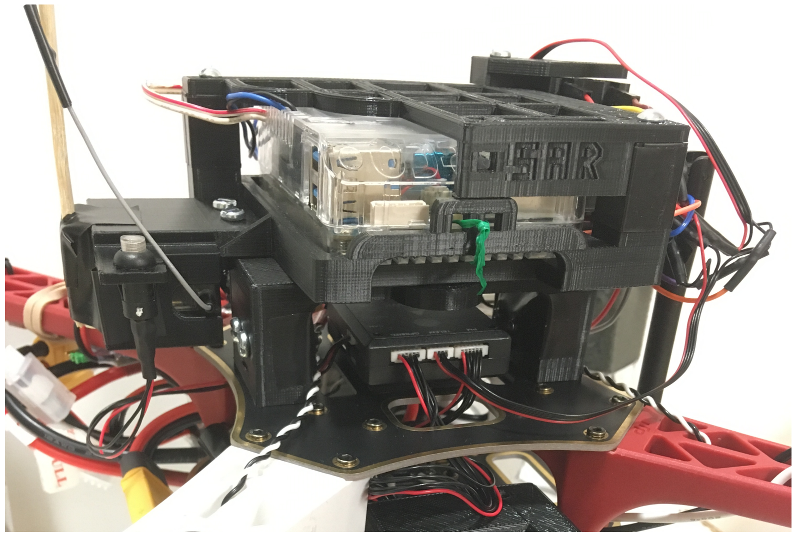

Figure 3.13: The design is modular and compact, yet still facilitates airflow for cooling. In the event of a crash, the mounts are usually the first point of failure, absorbing the blow and protecting the other components.

3.3 Summary

Table 3.1 shows the major hardware components associated with the final implementation of the search-and-rescue system. Minor low-cost components such as cables and the wireless network antenna are largely interchangeable and thus not listed. Recommendations for future implementations are discussed in greater detail in Chapter 6.

Table 3.1: Final system implementation

Component	**Part Selection**	**Cost**
Frame	DJI F450 kit	$190
Motors	DJI 2312e	Inc.
ESCs	DJI 430 Lite	Inc.
Propellers	DJI 9450	Inc.
Battery	Tattu 1800mAh 3s 75c LiPo (x2)	$48
Radio	Radiolink AT9S	$106
Flight Controller	3DR Pixhawk Mini	$160
GPS	3DR Micro M8N	Inc.
Telemetry	Holybro Micro FPV Telemetry	Inc.
Power Module	Holybro APM 10s	$22
UBEC	HENGE 6V 6A	$14
SBC	Odroid XU-4	$60
VPU	Intel NCS2	$88
Camera	GoPro Hero 6 Refurbished	$280
Man-in-the-middle	Teensy 3.1	$20
Total		**$988**

Chapter 4

System Software

Three main versions of the search-and-rescue (SAR) program were developed, each with different objectives in mind. Section 4.1 explores the initial program, designed to implement off-the-shelf models with the NCSDK API. Section 4.2 explores the second iteration of the program, which attempts to compensate for weaknesses in these models through methods such as alternating detection windows. Section 4.3 explores the final program, which utilizes a custom-trained model and the OpenVINO API and demonstrates superior recall and performance.

4.1 SAR1

The NCSDK API was installed on the Odroid and utilized for deployment of off-the-shelf pre-trained models from the Movidius Model Zoo [32]. Both TinyYolo [33] and a Mobilenet SSD [34] were explored. Frames are read at a constant, user-specified rate by the FFMPEG tool and logged locally. The program pulls the latest frame off the top of the stack, performs inference, and logs the results locally. The finite state machine (FSM) is shown in Fig. 4.1.

While this method is simple and effective, it results in unnecessary overhead on the Odroid. For bench testing purposes, an alternate method was

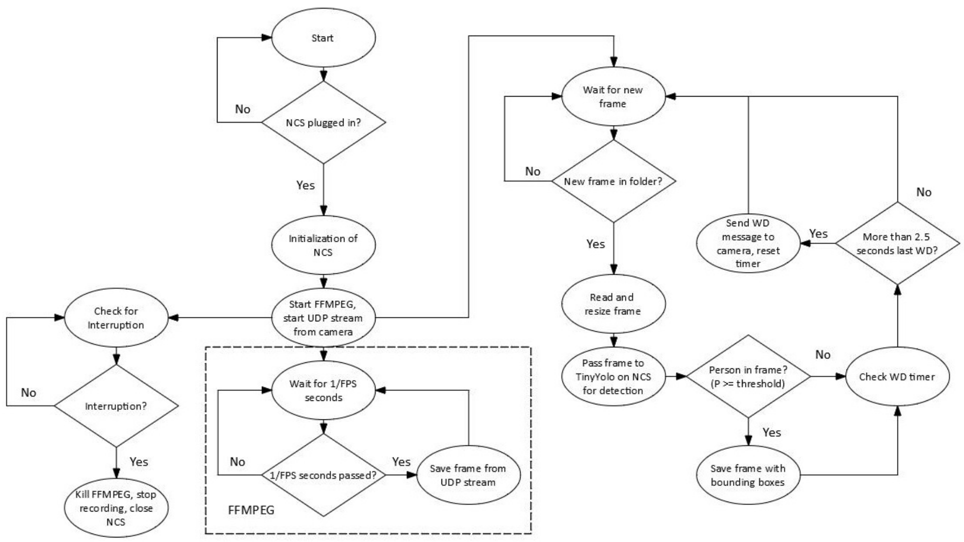

Figure 4.1: Initial SAR1 code FSM

written to feed pre-extracted frames from a test video to the SAR program at a constant rate. The program was further improved through the implementation of a threaded architecture, as shown in Fig. 4.2. This allows the Odroid to prepare the next frame while inference is still being executed on the previous frame; because that inference occurs on the NCS rather than the SBC, there is no performance penalty as the SBC would otherwise be waiting in an idle state anyways.

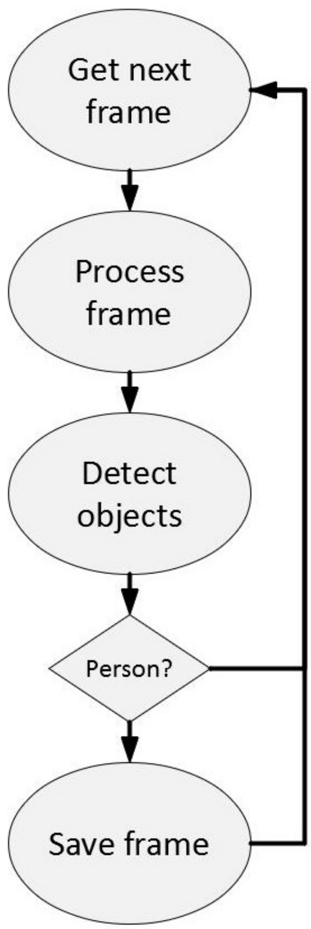

(a) Non-threaded architecture (entirely linear process)

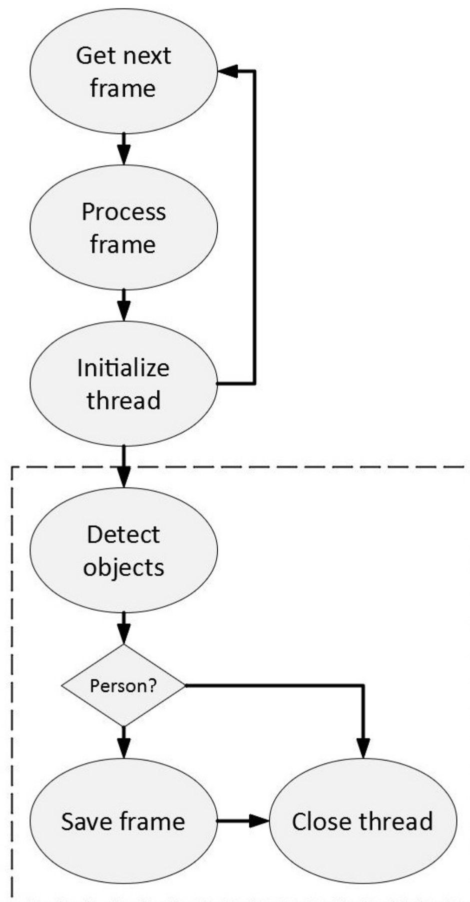

(b) Threaded architecture (thread surrounded by dashed box)

Figure 4.2: Non-threaded vs threaded architecture

4.2 SAR2

The primary goal of the SAR2 program was to stretch the off-the-shelf models to their limits by optimizing the rest of the code as musch as possible. Instead of the local logging and reading of frames, an OpenCV video stream directly from the camera feed was employed. In addition, frames were preprocessed in a "flashing window" fashion that alternated between cropping off the right or left sides of the frame on subsequent calls. At this point, Mobilenet SSD support was dropped to focus on TinyYolo, as the latter exhibited better recall on test videos. Fig. 4.3 shows the updated FSM for this process, while Fig. 4.4 demonstrates how the flashing window selectively crops frames in consecutive operations.

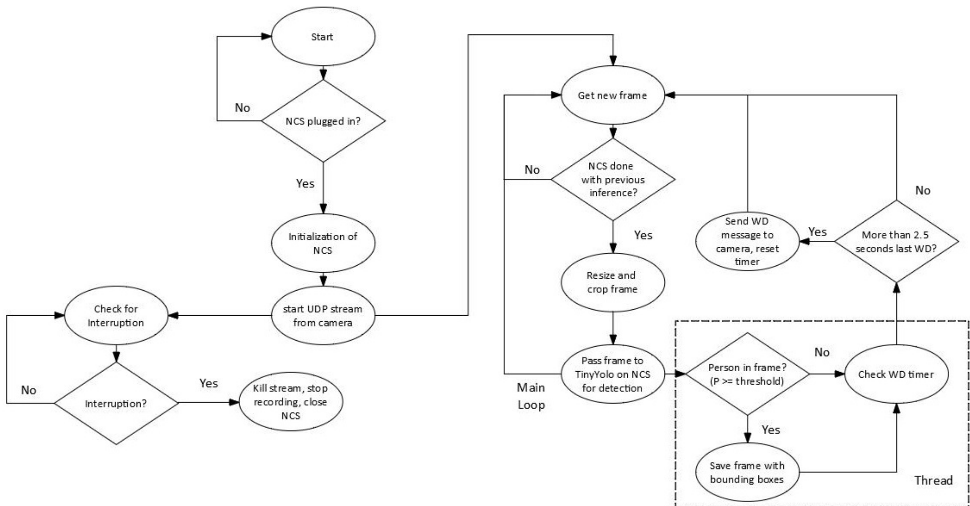

Figure 4.3: SAR2 code FSM

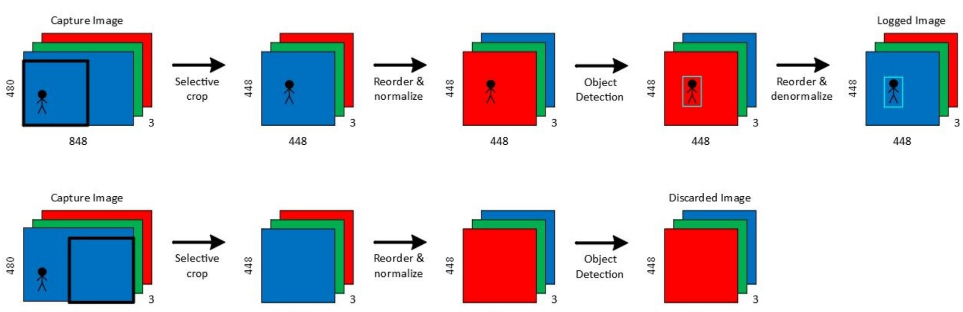

Figure 4.4: SAR2 flashing window method - note the reversal of BGR and RGB required before and after inference due to the image format of OpenCV

4.3 SAR3

The SAR3 program represents a substantial step forward from the previous versions, introducing support for the OpenVINO API and thus allowing networks to be deployed on the NCSv2 as well as the NCSv1. The original streaming backend implementation through FFMPEG was modified to instead utilize Gstreamer, in an attempt to rectify issues with the GoPro stream when using the new OpenCV version required by this build.

Instead of an off-the-shelf network, this implementation makes use of a custom-trained, single-class TinyYolo network dubbed "Dijon". Dijon resizes the anchor boxes of a typical TinyYolo model [33] to achieve better convergence at the task of subject identification. The network utilizes an 800x480x3 input layer that reduces to a 25x15 grid, where each grid space proposes five anchor boxes. The 848x480 feed of the GoPro therefore can be fed almost directly into the network. While the 24 pixels at either edge of the frame are discarded, because they are already prone to being occluded by the drone legs when in flight, the information loss is negligible. Fig. 4.5 shows the FSM for the final implementation.

4.3.1 Dataset

While several datasets focused on pedestrian detection are readily available, such as the Caltech Pedestrian dataset [20], most are shot from street level and thus not well suited for training a network to classify from the air. A notable exception is the Okutama-Action dataset, featuring over 60,000 frames

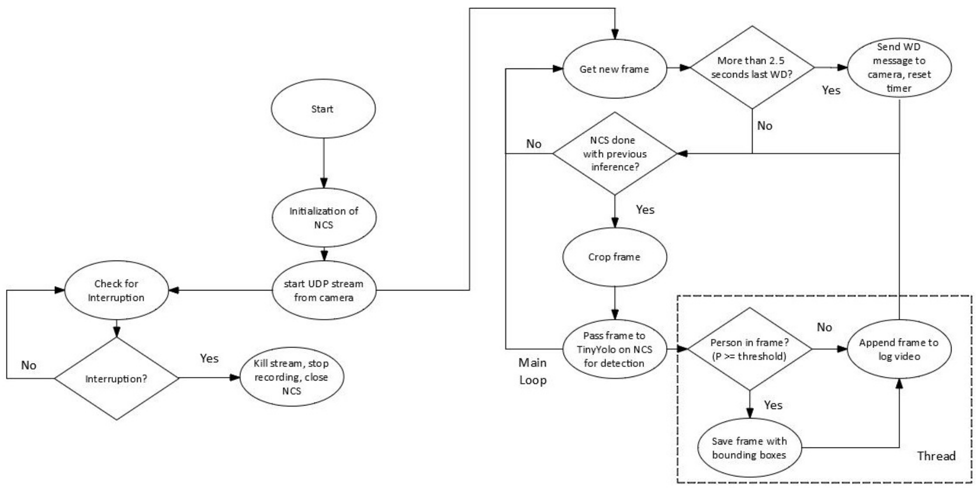

Figure 4.5: SAR3 code FSM

of labelled action data filmed with a drone [21].

Albatross

The Okutama-Action dataset was augmented with labelled frames from a video recorded onboard the drone (Section 5.2.1). The resulting dataset, dubbed "Albatross", was further improved via the addition of negative (ground truth zero) frames showing objects that commonly caused false positives with Okutama-Action, such as automobiles in a parking lot. Altogether, the use of the Albatross class adds about 7100 additional samples. Fig. 4.6 shows a selection of sample images from the two datasets.

(a) Samples from Okutama-Action

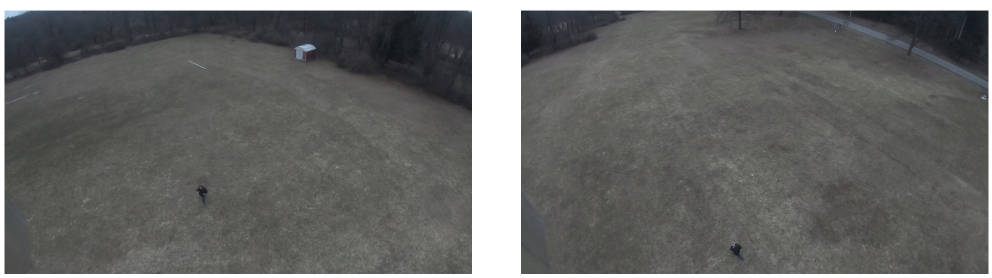

(b) Samples from Albatross

Figure 4.6: Select images from training dataset

4.3.2 Training

The network was trained using the Darknet framework via dual Nvidia Titan V GPUs. Firstly, a high-resolution 1280x720 network ("Cherry") was trained on the dataset for 120,000 batches, using the Tiny YOLOv2 VOG weights for initialization. Next, the Cherry weights were used by a 800x480 network ("Mustard") to perform transfer learning for 120,000 batches. Finally, the Mustard weights were trained for another 150,000 batches, resulting in the "Dijon" network. For Dijon, Darknet dataset augmentation parameters such as saturation and hue variance were scaled to twice their typical values, thus subjecting the network to a wider variety of input images. The learning rates were updated in accordance with the schedule shown in Table 4.1.

Table 4.1: Learning rate hyperparameters for network training.

Iterations	**Learning Rate**		
	Cherry	Mustard	Dijon
0	0.001	0.001	0.0001
50,000	0.0005	0.0005	0.00005
65,000	0.0001	0.0001	0.00001
80,000	0.00001	0.00001	0.000001

4.3.3 Deployment

For use with the NCS, the Darknet model was first converted to a Tensorflow model via Darkflow [35]. The result was then converted to the OpenVINO Intermediate Representation format using the OpenVINO Model Optimizer program, resulting in ".bin" and ".xml" files to be deployed for inference.

Chapter 5

Results

5.1 Bench Testing

5.1.1 Off-the-shelf model performance

A threaded architecture is utilized to test the throughput of both the Mobilenet SSD and of TinyYolo on the NCSv1. The effects of using different devices and ports are explored, as summarized in Table 5.1. The inference time (Inf) is characteristic of the NCS itself, whereas the "function" time (Func) takes into account the delay associated with transferring data on and off the device and is thus system-dependent. The data clearly demonstrate the superiority of the Odroid over the Raspberry Pi 3B used by Szankin [22] and Hochstetler et al. [27].

Table 5.1: Comparison of throughput for off-the-shelf networks

Task	**Pi 3B (USB2)**		**Odroid (USB2)**		**Odroid (USB3)**	
	Time (ms)	FPS	Time	FPS	Time	FPS
Mobilenet Inf	88.32	11.32	88.32	11.32	88.32	11.32
Mobilenet Func	140.84	**7.100**	130.95	**7.637**	112.58	**8.883**
TinyYolo Inf	124.02	8.063	124.02	8.063	124.02	8.063
TinyYolo Func	223.70	**4.470**	205.49	**4.866**	165.61	**6.038**

5.1.2 Custom Model Performance

Table 5.2 shows the average bench performance of the Dijon network when tested with both versions of the NCS and both types of USB ports. The network is able to beat the best TinyYolo results from 5.1 despite having nearly twice the parameter count due to its larger input size (800x480 vs 448x448). Furthermore, it is shown in field tests to exhibit vastly improved recall and precision as compared to the off-the-shelf TinyYolo model. The network was also deployed using the NCSDK and NCSv1 and found to achieving 2.9637 FPS over USB3. This validates the advertised superior performance of the OpenVINO API over the older NCSDK.

Table 5.2: Dijon throughput test results

Stick	USB Port	Latency (ms)	FPS
NCSv1	2.0	368.4170	2.7143
NCSv1	3.0	281.7030	3.5498
NCSv2	2.0	217.2030	4.6040
NCSv2	3.0	115.6840	8.6442

5.2 Field Testing

The system design was verified to be effective at the task of detecting missing persons through the performance of field tests at a public park. Actors were recruited to pose around the edges of a field. The drone autonomously executed a pre-programmed mission (shown in Fig. 5.1) to traverse the field, a total flight distance of 0.587 km. An operator on the ground controlled the yaw of the drone to keep it pointing towards the closer edge of the field. It

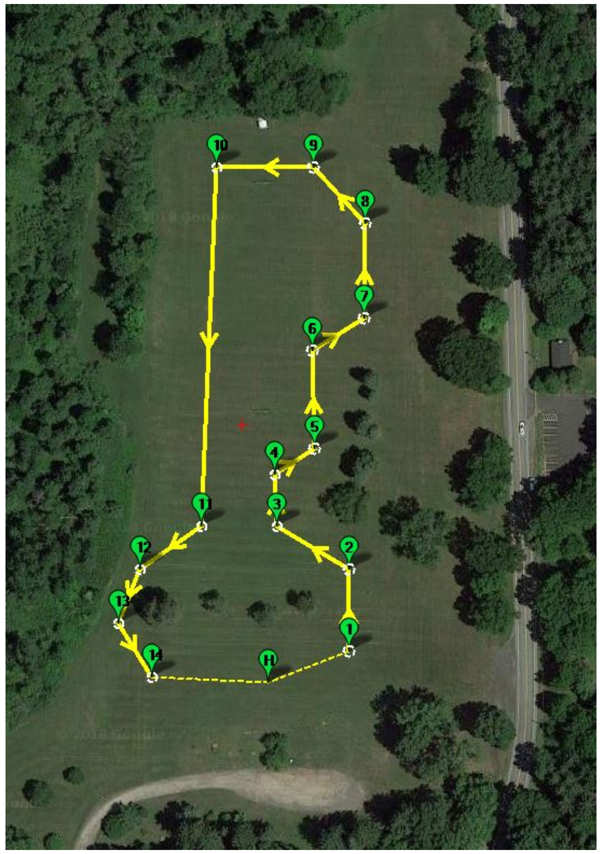

Figure 5.1: Mission waypoints assigned for field testing

should be noted that "ROI" mission commands can also be used to redirect the drone to face a "region of interest", meaning this oversight role could be eliminated through more complex mission design. Test flights were performed to explore each of the different SAR program versions (Section 4).

5.2.1 SAR1 flight tests

Field tests were performed on two separate occasions to explore the effectiveness of the off-the-shelf TinyYolo model with the SAR1 architecture. A fixed value of 5 FPS was utilized for the streaming rate.

Winter flight

A flight was attempted to explore the effects of a snowy backdrop on the detector recall. While conditions were windless, the temperature was near freezing, resulting in difficulties with the NCS becoming too cold and shutting down. These were initially addressed by attaching hand warmers to the frame near the device. The decision was made to fly regardless in order to accumulate video samples for offline analysis on the bench later. Shortly after the drone passed Waypoint 8 (Fig. 5.1), a complete power failure occurred and it fell some 15-20 feet out of the sky, bringing the test flight to a rapid end.

Solo flight

Several weeks after the winter flight, another flight was attempted in more hospitable conditions. Instead of utilizing actors along the search path, for this test the operator ran ahead of the drone as the person to be detected. The drone was able to fly between all of the assigned waypoints completely autonomously and successfully land on its own afterwards. Detection was performed offline due to connectivity issues between the Odroid and GoPro. Even though the operator appeared in approximately two-thirds of the total

Figure 5.2: Results from Solo flight of SAR1 test flights

frames, only a single successful detection was observed with the TinyYolo network (Fig. 5.2, confidence 0.12356).

Outcome

The major crash of the winter flight shattered most of the mounts and two propellers, but seemingly spared the other components. The cause of the crash was traced back to a faulty switch used to isolate the batteries; the contacts must have separated in-flight, resulting in a complete loss of power. In addition to the replacement of this switch, the crash prompted a nearly complete systems teardown and extensive redesign of the mounting components. While the previous mount iteration had focused on having minimizing complexity, the new mounts (shown in Section 3.2) favored a modular design that allows components to be swapped out without requiring a full mount reprint. It is suspected that some GPS and radio issues encountered later may be traced back to damage unknowingly sustained during the crash. The flight did yield video samples of subjects that later proved useful for bench testing.

Despite the underwhelming recall of the solo flight, the test was a major success in two regards. Firstly, it demonstrated the feasibility of an entirely autonomous search operation through the use of assigned waypoints as an autopilot mission. Secondly, it yielded excellent video of a human subject at altitude and angle desired for the final application. This footage would later be labelled and used to create the Albatross dataset (Section 4.3.1).

5.2.2 SAR2 flight tests

A field test was performed to test the performance of off-the-shelf TinyYolo with the SAR2 program. The same autopilot mission used for the SAR1 tests constituted the intended flight path. Two flights were attempted back-to-back; the first under cloudy but windless conditions, the second with occasional wind gusts. The NCSv1 was utilized for inference, achieving an average of 5.732 FPS on the 448x448 resolution network.

Flight 1

Almost immediately after takeoff, the drone lost radio contact with the operator controller. In accordance with its safety settings (implemented to prevent flyaways), it performed an automated landing and ended the mission. A successful detection was recorded, as shown in Fig. 5.3 (confidence 0.07903).

Figure 5.3: Results from Flight 1 of SAR2 test flights

Flight 2

The drone was rebooted and rearmed in anticipation of a second flight. This flight began with a successful navigation of the first few waypoints and the detection of an actor and the operator, as shown in Fig. 5.4. However, a low battery warning soon triggered abruptly, resulting in an automated emergency landing. Shortly afterwards, the weather shifted and a drizzle began; as such, further attempts at testing were discontinued to protect the drone hardware and Odroid from damage.

(a) Actor 1, Confidence 0.08558

(b) Operator, Confidence 0.14020

Figure 5.4: Select results from Flight 2 of SAR2 test flights

Outcome

While the system was able to successfully detect actors, the network recall was quite poor. For most of the frames in which an actor appeared, the detection confidence was below the SAR2 threshold of 7%, as is clearly visible in Fig. 5.3. The test served to reinforce the need for a higher-resolution subject detector. It also marked the first appearance of what would be a recurring but intermittent issue in which the controller and drone would lose communication, resulting in an emergency landing. While in an actual search-and-rescue operation such a failsafe would be disabled, the system reliability did not yet inspire enough confidence for it to be disabled in this implementation. The battery-related issue was explored on the bench after the test and discovered to be caused by an offset issue with the voltage monitor. It was addressed by tweaking the battery failsafe threshold parameter. Finally, the test exposed the need for a more weather-proof enclosure for the Odroid and sensitive electrical components in future implementations.

5.2.3 Final flight tests

A final field test was undertaken to test the field performance of the Dijon network with the SAR3 program. The autopilot mission was assigned to the same "key" flight path utilized in earlier tests (Fig. 5.1). Four actors were recruited to follow the paths and undertake the actions specified in Fig. 5.5. Two flights, with a short break between them, were performed around 8AM under clear and largely windless flight conditions. The NCSv2 was utilized for inference, achieving an average of 7.601 FPS on the 800x480 resolution network.

Flight 1

At the test site, the GPS was unable to achieve a satisfactory lock due to EKF variance. Therefore, the auto mode was not utilized, and the drone was instead flown under manual control by the operator, approximating the intended flight path. The system was able to successfully identify all four actors, as shown in Fig. 5.6, even with difficult background conditions such as glare and shadows from the early-morning sun.

Unfortunately, due to a typo in a late revision to the SAR3 program, when the bounding boxes for the detected persons were to be overlaid on the cropped inference image for local logging the non-cropped image was inadvertently utilized instead. Therefore, the bounding boxes were offset by 24 pixels to the

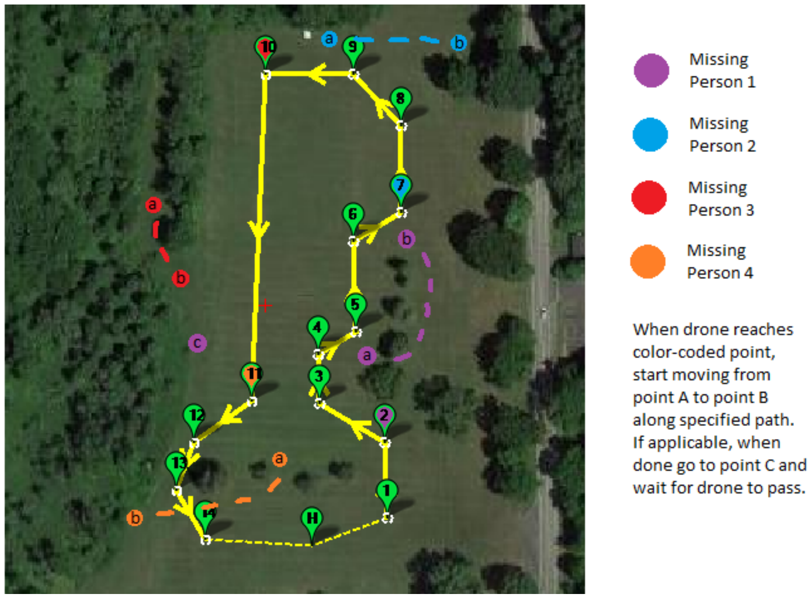

Figure 5.5: Actors' script for final flight test

left, and thus appear slightly erroneous despite the successful performance of the network.

Flight 2

After the aforementioned bounding box offset bug was addressed, a second test flight was initiated. Once again, the GPS failed to achieve a lock, so the drone was flown along the specified path under manual operator control. Shortly after takeoff, the low battery alarm was triggered and an automated emergency landing performed. Measurement of the main battery voltage on the bench would later show it had dropped to 10.58V, having already powered the system for a full flight as well as for initialization tasks on the ground. As the Odroid and NCS were still successfully performing inferences, the main

(a) Actor 1, Confidence 0.43872

(b) Actor 2, Confidence 1.0

(c) Actor 3, Confidence 0.29419

(d) Actor 3, Confidence 0.48975

(e) Actor 3, Confidence 0.50195

(f) Actor 4, Confidence 0.28735

Figure 5.6: Select results from Flight 1 of Final test flights

(a) Actors 1 and 2, Confidence 0.96875

(b) Actor 1, Confidence 0.26782

(c) Actor 2, Confidence 1.0

(d) Actor 2, Confidence 1.0

Figure 5.7: Select results from Flight 2 of Final test flights

battery was quickly swapped with a backup battery and the flight resumed. Thereafter, the system was able to successfully identify Actors 1 and 2, as shown in Fig. 5.7.

Near Waypoint 9 (Fig 5.1), the drone unexpectedly lost contact with the radio controller. As such, an automated emergency landing was once again triggered. Attempts to fix the issue by rebooting the flight controller and associated subsystems proved fruitless, and the flight was ended before Actors 3 and 4 were reached. When the drone was later tested on the bench, the controller and drone were able to communicate successfully, suggesting the cause was the same intermittent problem observed in previous test flights.

Outcome

The system struggled to identify actors at great distances from the camera, as shown in Fig. 5.6c. However, it succeeded at its primary goal by identifying each actor at their assigned location, in many cases with extremely high confidence. This was accomplished despite the incredibly low stream quality of the GoPro when used with OpenCV 4, as required by the SAR3 build. While the test proves the efficacy of the Dijon network in the field, it also provides a strong incentive for a different camera (preferably hardwired) to be utilized in future applications. The test also demonstrated the increased unreliability of the system after having endured many rough landings and crashes (including several "yard" tests not reported here), suggesting a "fresh" drone might exhibit more consistency.

Chapter 6

Conclusions

By the end of the testing process, the drone implemented here had suffered a number of failures and crashes. Most of these could be traced to operator error or to the use of faulty components that in future builds could easily be avoided. It is possible that the root cause of other issues could also be traced back to earlier crash events and mishaps. For example, the intermittent loss of flight controller communication is likely due to an incident early in the development process in which the last half inch of the antenna was chopped off by the propellers (due to ill-advised mounting and an unexpectedly sensitive throttle response). Therefore, while the system durability could theoretically present an issue in future implementations, a freshly assembled drone with new components would be unlikely to experience these issues.

If the specific unit implemented here were to be reused, several changes are recommended. It is suggested the cabling between the flight controller and radio be replaced, the radio antenna (or even the entire receiver and transmitter) replaced, the GoPro replaced with a hardwired camera, and the GPS mounted on a raised mast above the drone for improved signal quality. A single battery supported about 8-10 minutes flight time, and two batteries supported about 17 minutes; for increased flight time, the batteries should be replaced with a single high-capacity battery.

While the GoPro is not recommended for future implementations, it was an appropriate component selection for this proof-of-concept implementation. It is unlikely that many other cameras would have survived the abuse endured by the unit across the multiple rough landings and crashes associated with the development process. The main reason the GoPro is advised against is going forward is its seeming incompatibility with OpenCV 3 and 4 (which are required to make use of the OpenVINO API). This is despite the fact that the camera worked nearly flawlessly with OpenCV 2. It is possible that building the FFMPEG tool from the source might solve this problem, although the fact that the similar Gstreamer tool also proved an unreliable means of loading the stream suggests a deeper incompatibility.

The use of a full-size Pixhawk is recommended for future swarm-oriented builds, as it better facilitates access to the FC via UART. This would allow for simple MAVLink communication between the FC and onboard SBC via an FTDI cable. The SBC could thus easily exert control over the FC, allowing the adjustment of wavepoints "on the fly". For example, if a person were detected with a medium degree of certainty, the SBC could instruct the autopilot to deviate from its planned course to investigate the potential sighting up close.

Before the system is put into service and deployed in the field for high-stakes search operations, it is suggested that an operator perform controlled flights around the deployment area and record video under various lighting and environmental conditions. Frames from these videos could be used to fine-tune the missing person detection network for the expected terrain, reducing the likelihood of false positives. Additional improvements such as support for

Table 6.1: Proposed future implementation

Component	**Part Selection**	**Cost**
Frame	F450 clone	$19
Motors	DJI 2312e	$99
ESCs	DJI 430 Lite	Inc.
Propellers	DJI 9450	Inc.
Battery	Tattu 4200mAh 3s 35c LiPo	$48
Radio	DXe DSMX 2.4Ghz Sport	$90
Flight Controller	Holybro Pixhawk 2.4.6	$180
GPS	Holybro M8N	Inc.
Telemetry	Holybro 100mW Telemetry	Inc.
Power Module	Holybro APM 10s	Inc.
UBEC	HENGE 6V 6A	$14
SBC	Odroid XU-4	$60
VPU	Intel NCS2	$88
Camera	Logitech C270	$40
Total		**$638**

multiple classes could be implemented to permit the observation of wildlife or tracking of trespassing vehicles, as in [36].

Table 6.1 provides a recommended components list for future builds. Two such implementations could be assembled for less than the price of an entry-level off-the-shelf system [37]. Alternatively, a single implementation could provide a low-cost base upon which other, more expensive components such as thermal cameras or a real-time kinematic (RTK) GPS could be added for improved system efficacy.

Chapter 7

Future Work

The most immediate possible extension of this work is the construction of a second drone and implementation of synchronized search of an area. Automatic segmentation and traversal of a search polygon, similar to [1], could be implemented. Drone-to-drone communication should be considered. Once two drones have been implemented as proof-of-concept, the system may be scaled up to support a larger swarm.

The Dijon network recall, while impressive, could be further improved augmenting the Albatross dataset with more samples at various distances and angles, with actors in various clothing and positions. Additionally, negative samples that include camera noise and dense woods should be used, as these have been observed to trigger false positives. A secondary recurrent network could be implemented to wrap the output of the Dijon detector and distinguish true positives from false positives. The use of multiple NCSv2 devices through a powered USB hub could be explored, as could the use of alternative accelerator solutions such as an Nvidia Jetson Nano.

Bibliography

[1] A. M. de Oca, L. Arreola, A. Flores, J. Sanchez, and G. Flores. Low-cost multispectral imaging system for crop monitoring. *International Conference on Unmanned Aircraft Systems (ICUAS)*, 2018.

[2] A. Rivera, A. Villalobos, J. Monje, J. Marinas, and C. Oppus. Post-disaster rescue facility: Human detection and geolocation using aerial drones. *IEEE Region 10 Conference (TENCON)*, 2016.

[3] M. H. Dominguez, S. Nesmachnow, and J. Hernndez-Vega. Planning a drone fleet using artificial intelligence for search and rescue missions. In *IEEE XXIV International Conference on Electronics, Electrical Engineering and Computing (INTERCON)*, 2017.

[4] S. Bernardini, M. Fox, and D. Long. Planning the behaviour of low-cost quadcopters for surveillance missions. In *International Conference on Automated Planning and Scheduling (ICAPS)*, 2014.

[5] M. Modasshir, A. Quattrini Li, and I. Rekleitis. Deep neural networks: A comparison on different computing platforms. In *15th Conference on Computer and Robot Vision (CRV)*, 2018.

[6] S. Rivas-Gomez, A. Pena, D. Moloney, E. Laure, and S. Markidis. Exploring the vision processing unit as co-processor for inference. *2018 IEEE International Parallel and Distributed Processing Symposium Workshops (IPDPSW)*, 2018.

[7] T. Heggie and M. Amundson. Dead men walking: Search and rescue in US National Parks. *Wilderness and Environmental Medicine*, 2009.

[8] T. Sharples. Get into trouble outdoors - who pays for the rescue? *Time*, 2009.

[9] David McKie. Search and rescue for false alarms costs millions. *CBC News*, 2014.

[10] DJI, Black Channel, and EENA. Drone efficacy study - evaluating the impact of drones for locating lost persons in search and rescue events. *European Emergency Number Association (EENA)*, 2018.

[11] H. Saha, S. Basu, S. Auddy, R. Dey, A. Nandy, D. Pal, N. Roy, S. Jasu, A. Saha, S. Chattopadhyay, and T. Maity. A low cost fully autonomous gps (global positioning system) based quad copter for disaster management. In *IEEE 8th Annual Computing and Communication Workshop and Conference (CCWC)*, 2018.

[12] R. Tariq, M. Rahim, N. Aslam, N. Bawany, and U. Faseeha. Dronaid: A smart human detection drone for rescue. In *15th International Conference on Smart Cities: Improving Quality of Life Using ICT & IoT (HONET-ICT)*, 2018.

[13] S. Lee, D. Har, and D. Kum. Drone-assisted disaster management: Finding victims via infrared camera and lidar sensor fusion. *3rd Asia-Pacific World Congress on Computer Science and Engineering*, 2016.

[14] G. Bevacqua, J. Cacace, A. Finzi, and V. Lippiello. Mixed-initiative planning and execution for multiple drones in search and rescue missions. In *25th International Conference on International Conference on Automated Planning and Scheduling (ICAPS)*, 2015.

[15] L. Baumgrtner, A. Penning, P. Lampe, B. Richerzhagen, R. Steinmetz, and B. Freisleben. Environmental monitoring using low-cost hardware and infrastructureless wireless communication. In *IEEE Global Humanitarian Technology Conference (GHTC)*, 2018.

[16] S.A. Celtek, A. Durdu, and E. Kurnaz. Design and simulation of the hierarchical tree topology based wireless drone networks. In *International Conference on Artificial Intelligence and Data Processing (IDAP)*, 2018.

[17] Y. Ganesh, R. Raju, and R. Hegde. Surveillance drone for landmine detection. *International Conference on Advanced Computing and Communications (ADCOM)*, 2015.

[18] H. Kayan, R. Eslampanah, F. Yeganli, and M. Askar. Heat leakage detection and surveiallance using aerial thermography drone. *26th Signal Processing and Communications Applications Conference (SIU)*, 2018.

[19] T. Giitsidis, E.G. Karakasis, A. Gasteratos, and G. Ch. Sirakoulis. Human and fire detection from high altitude uav images. In *23rd Euromicro International Conference on Parallel, Distributed, and Network-Based Processing*, 2015.

[20] P. Dollar, C. Wojek, B. Schiele, and P. Perona. Pedestrian detection: A benchmark. In *The IEEE Conference on Computer Vision and Pattern Recognition (CVPR)*, 2009.

[21] M. Barekatain, M. Mart, H. Shih, S. Murray, K. Nakayama, Y. Matsuo, and H. Prendinger. Okutama-action: An aerial view video dataset for concurrent human action detection. In *The IEEE Conference on Computer Vision and Pattern Recognition (CVPR) Workshops*, 2017.

[22] M. Szankin, A. Kwaniewska, J. Ruminski, and R. Nicolas. Road condition evaluation using fusion of multiple deep models on always-on vision processor. In *IECON 2018 - 44th Annual Conference of the IEEE Industrial Electronics Society*, Oct 2018.

[23] D. Hou, T. Liu, Y. Pan, and J. Hou. AI on edge device for laser chip defect detection. In *IEEE 9th Annual Computing and Communication Workshop and Conference (CCWC)*, 2019.

[24] Intel. Intel movidius myriad 2 vpu enables advanced computer vision and deep learning features in ultra-compact dji spark drone. 2017. `https://www.movidius.com/news/intel-movidius-myriad-2-vpu-enables-advanced-computer-vision-and-deep-learn`.

[25] A. Boka and B. Morris. Person recognition for access logging. In *IEEE 9th Annual Computing and Communication Workshop and Conference (CCWC)*, 2019.

[26] I. Lobachev, R. Maleryk, S. Antoschuk, D. Filiahin, and M. Lobachev. Integration of neural networks into smart sensor networks. In *2018 IEEE 9th International Conference on Dependable Systems, Services and Technologies (DESSERT)*, May 2018.

[27] J. Hochstetler, R. Padidela, Q. Chen, Q. Yang, and S. Fu. Embedded deep learning for vehicular edge computing. In *2018 IEEE/ACM Symposium on Edge Computing (SEC)*, Oct 2018.

[28] DJI. E305 user manual. `http://dl.djicdn.com/downloads/e305/en/E305_User_Manual_v1.00_en.pdf`.

[29] Hardkernel. Odroid xu4. `https://www.hardkernel.com/shop/odroid-xu4`.

[30] Intel. Neural compute stick. `https://software.intel.com/en-us/movidius-ncs`.

[31] Intel. Neural compute stick 2. `https://software.intel.com/en-us/neural-compute-stick`.

[32] Movidius. Neural compute application zoo. `https://github.com/movidius/ncappzoo`.

[33] J. Redmon and A. Farhad. Yolo9000: Better, faster, stronger. *arXiv preprint arXiv:1612.08242*, 2016.

[34] A. G. Howard, M. Zhu, B. Chen, D. Kalenichenko, W. Wang, T. Weyand, M. Andreetto, and H. Adam. Mobilenets: Efficient convolutional neural networks for mobile vision applications. *arXiv preprint arXiv:1704.04861*, 2017.

[35] thtrieu. Darkflow. `https://github.com/thtrieu/darkflow`.

[36] Susan Gawlowicz. Cracking down on poachers with imaging. 2019. `https://www.rit.edu/news/cracking-down-poachers-imaging`.

[37] D. Wheeler. Search and rescue drones catalog. 2019. `https://www.dslrpros.com/sar-drones.html`.